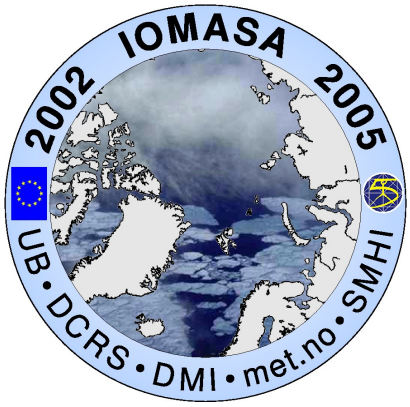

IOMASA Deliverable 3.1.1:

A Forward Model

For Calculating The AMSR Brightness Temperatures

Of Sea-ice And Ocean

As Seen Through The Atmosphere.

Dorthe Hofmann-Bang

Leif Toudal Pedersen

Danish Center for Remote Sensing

Ørsted*DTU

Technical University of Denmark

2003

1 Abstract

This report describes a forward model for open water and the atmosphere, and how the contribution from sea ice can be included in these. In addition the report describes a retrieval algorithm that allows validation of the forward model. The model and the algorithm are verified by comparison with SSM/I retrievals, with ocean and atmosphere retrievals by Remote Sensing Systems, with SST data from the Ocean and Sea Ice SAF and with sea ice concentrations and MY-fractions of the NASA Team and Comiso Bootstrap sea ice algorithms. The forward model is the level 0 emissivity and radiative transfer model for the IOMASA project.

2 Introduction

With the AMSR satellite microwave radiometer on-board the EOS-AQUA satellite it is possible to obtain long time series of brightness temperatures over sea-ice and ocean. From the brightness temperatures, geophysical parameters important for studying the global hydrologic cycle and the Earth's radiation budget, can be retrieved. The parameters, which can be retrieved, are two of the three phases of atmospheric water – vapor and liquid. Furthermore, surface parameters such as the near-surface wind speed, the sea surface temperature, the sea ice concentration and the sea ice type can be retrieved.

This document describes a forward model, which relates the geophysical parameters to brightness temperatures measured by the AMSR. The forward model for open water/atmosphere is described by Wentz 2002. In the present document it is explained how the model can be expanded so it also includes ice covered surfaces. Next, the document describes a statistical method on how the geophysical parameters can be retrieved from the measured brightness temperatures. Then, the document includes a section on how the model has been verified and a section with some examples of the use of the retrieval algorithm. Finally the document ends with a summary of the results obtained by the examples and a discussion of the results.

3 Theory

3.1 Forward Model

Radiative transfer theory provides the relationship between the observed brightness temperatures T_B (K) and some geophysical parameters. A model describing this relationship is known as a forward model, and here a forward model described by Wentz 2002 has been used. The model describes the connection between 4 geophysical parameters (wind, water vapor, liquid water and sea surface temperature) and the brightness temperatures measured by the AMSR. The model described by Wentz 2002 is only valid for water surfaces, so the model has to be expanded to take ice covered surfaces in to account.

3.1.1 Inclusion of ice in the Forward Model

In the model by Wentz 2002 the upwelling brightness temperature at the top of the atmosphere - the brightness temperature measured by the AMSR satellite - is written in equation (10) as:

$$T_{B\uparrow} = T_{BU} + \tau\left[ET_S + T_{B\Omega}\right]$$

where T_{BU} is the contribution of the upwelling atmospheric emission, τ is the total transmittance from the surface to the top of the atmosphere, E is the Earth surface emissivity and $T_{B\Omega}$ is the surface scattering integral.

A change in the surface content from open water to ice only have an influence on the following parts of the model: ET_s (the brightness temperature close to the sea surface) and $T_{B\Omega}$.

In order to be able to include ice in the model for the brightness temperature close to the sea surface, one has to consider the difference between the emissivity of an open water sea surface and an ice covered sea surface.

The brightness temperature, $T_{B,ice}$, at the ice surface can be written as:

$$T_{B,ice} = T_{p,ice} \cdot E_{ice}$$

where $T_{p,ice}$ is the physical temperature of the ice surface and the E_{ice} is the emissivity of the ice surface.

The emissivity of an ice covered surface is dependant on the type of ice cover, the polarization and the frequency. The sea ice emissivities used to calculate the brightness temperatures of the different channels of the AMSR are given in the Table 3-1. Table 3-1a gives typical values for the Fall of 2003 (September-November) and Table 3-1b gives values for the Winter 2003-04 (November-April).

Freq		6GHz	10GHz	18GHz	23GHz	37GHz
FY	Vertical	0.9204	0.9127	0.9373	0.9409	0.9347
	Horizontal	0.7502	0.7738	0.8314	0.8490	0.8600
MY	Vertical	0.9692	0.9284	0.8843	0.8554	0.7813
	Horizontal	0.8651	0.8356	0.7917	0.7792	0.7248

Table 3-1a The table shows the emissivities for the First Year (FY) and Multi Year (MY) ice used in the forward model (Fall 2003).

Freq		6GHz	10GHz	18GHz	23GHz	37GHz
FY	Vertical	0.9905	0.9718	0.9817	0.9773	0.9567
	Horizontal	0.9097	0.9007	0.9072	0.9075	0.8927
MY	Vertical	0.9870	0.9487	0.8933	0.8494	0.7473
	Horizontal	0.8866	0.8627	0.8163	0.7871	0.7011

Table 3-2b The table shows the emissivities for the First Year (FY) and Multi Year (MY) ice used in the forward model (Winter 2003-04).

Now, the brightness temperature close to a surface mixed of open water, FY and MY ice can be written as:

$$T_{B,S} = ET_S = C_{ow}T_{B,ow} + C_{FY}T_{B,FY} + C_{MY}T_{B,MY}$$

where C_{FY}, C_{MY} and C_{ow} are the concentrations of open water and sea ice, and $T_{B,ow}$, $T_{B,FY}$ and $T_{B,MY}$ are the brightness temperatures of the three different surface types.

The surface scattering integral is given in Wentz 2002, equation (61) as:

$$T_{B\Omega} = \left[(1+\Omega)(1-\tau)(T_D - T_C) + T_C\right]R$$

In this equation it is only the sea-surface reflectivity R, which is influenced by the ice. An effective reflectivity for a mixed surface can be written as:

$$R_{eff,mix} = 1 - E_{eff,mix} = 1 - \left(C_{ow}E_{ow} + C_{FY}E_{FY} + C_{MY}E_{MY}\right)$$

where C_{ow}, C_{FY} and C_{MY} are the concentrations of the three surface types and E_{ow}, E_{FY} and E_{MY} are the emissivity of the surface types.

The last thing one has to take in to consideration, when including ice in the model, is that the forward model described by Wentz 2002 has a surface temperature included. This temperature has to take the temperature of the ice into account and therefore the surface temperature used in the ice model, has to be calculated by:

$$T_{S,mix} = C_{ice} \cdot T_{P,ice} + C_{ow} \cdot T_{P,ow}$$

where C_{ice} and C_{ow} is the concentration of open water and sea ice, and $T_{P,ice}$ and $T_{P,ow}$ are the surface temperatures. This mixed surface temperature only has to be used in the part of the model concerning the atmosphere, not in the parts concerning the dielectric constant of sea-water and the wind-roughened sea surface.

3.2 Inverse Model

The inverse model is used to retrieve the geophysical parameters from the brightness temperatures measured by the AMSR.
The inverse model used here is described by Rodgers 1976, and is based on an approximated linear function, which can be written in a discrete version as:

$$\mathbf{T_A} = \mathbf{Mp} + \mathbf{e}$$

where $\mathbf{T_A}$ is the brightness temperatures, **p** is the geophysical parameters, **e** is the normal distributed error with the covariance matrix $\mathbf{S_e}$ and **M** is the mixing matrix and contains the partial derivatives, and can be written as:

$$M_{ij} = \frac{\partial T_{Ai}}{\partial p_j}$$

A least square solution can be found for the linear function. The solution can be improved be including á priori information, and an expression for the estimated parameters, $\hat{p}$, can be written as:

$$\hat{\mathbf{p}} = \hat{\mathbf{S}}\left(\mathbf{S_p^{-1}p_0} + \mathbf{M^t S_e^{-1} T_A}\right)$$
$$\hat{\mathbf{S}} = \left(\mathbf{S_p^{-1}} + \mathbf{M^t S_e^{-1} M}\right)^{-1}$$

where $\hat{\mathbf{S}}$ is the covariance matrix of the estimated parameters, $\mathbf{S_p}$ is the covariance matrix of the á priori information and $\mathbf{p_0}$ is the mean values of the á priori information.
The equations are solved by using the method of Newtonian iteration. Newtonian iteration is described by Rodgers 1976 and is simply a matter of expanding the model as a Taylor series about a guessed value of the solution p_n. This can be written as:

$$\mathbf{p}_{n+1} = \mathbf{p}_n + \left(\mathbf{S}_p^{-1} + \mathbf{M}_n^T \mathbf{S}_e^{-1} \mathbf{M}_n\right)^{-1}\left(\mathbf{M}_n^T \mathbf{S}_e^{-1}\left(\mathbf{T}_A - \mathbf{T}_{A,n}\right) + \mathbf{S}_p^{-1}\left(\mathbf{p}_0 - \mathbf{p}_n\right)\right)$$

$\hat{\mathbf{p}}$ has been replace in the equation by p_{n+1} because this is an iterative equation , and $\mathbf{p_n} \to \hat{\mathbf{p}}$ as $n \to \infty$.

In order to be able to estimate the geophysical parameters the covariance matrix, $\mathbf{S_e}$ of the AMSR data and the á priori information has to be known. The covariance matrix of the measurements is showed in Table 3-3 (Reference: NASDA 2003).

	6V	6H	10V	10H	18V	18H	23V	23H	37V	37H
6V	0.09	0	0	0	0	0	0	0	0	0
6H	0	0.1089	0	0	0	0	0	0	0	0
10V	0	0	0.2209	0	0	0	0	0	0	0
10H	0	0	0	0.2916	0	0	0	0	0	0
18V	0	0	0	0	0.2304	0	0	0	0	0
18H	0	0	0	0	0	0.2116	0	0	0	0
23V	0	0	0	0	0	0	0.2025	0	0	0
23H	0	0	0	0	0	0	0	0.1936	0	0
37V	0	0	0	0	0	0	0	0	0.2025	0
37H	0	0	0	0	0	0	0	0	0	0.16

Table 3-3 The table shows the covariance matrix of the AMSR measurements. Reference: (NASDA 2003)

The á priori information used in the calculations is showed in Table 3-4 and Table 3-5. The covariance matrix has except for the sea ice temperature been calculated from a high resolution limited area model (HIRLAM). HIRLAM is a mesoscale atmospheric model operated at the Danish Meteorological Institute for analysis and forecast in the weather service. The data set covers the period from the 28th of March 2003 at 07.00 (UTC) to the 2nd of April 2003 at 05.00 (UTC). We have not been able to obtain any information about the sea ice temperature, and therefore the standard deviation (the diagonal elements in the covariance matrix) for the sea ice temperature has been set to the same value as the open water temperature. Furthermore because there is not á priori information about the sea ice temperature the off diagonal elements for the sea ice temperature have been set to 0.

Concerning the mean values, the first four values in the table has also been calculated from the HIRLAM data set. The last three values have been calculated by some simple algorithms, which are explained in the references.

	W	V	L	Tow	Tis	Cis	FMY
W	12.3024	3.2072	0.1398	6.0322	0	-0.6525	-0.9347
V	3.2072	11.0481	0.2495	11.9348	0	-0.3085	-0.5362
L	0.1398	0.2495	0.0204	0.2041	0	-0.0063	-0.0152
Tow	6.0322	11.9348	0.2041	23.9468	0	-0.7254	-1.0207
Tis	0	0	0	0	23.9468	0	0
Cis	-0.6525	-0.3085	-0.0063	-0.7254	0	0.0114	0.1203
FMY	-0.9347	-0.5362	-0.0152	-1.0207	0	0.1203	0.0332

Table 3-4 The table shows the covariance matrix for the á priori information.

W	V	L	Tow	Tis	Cis	FMY
4.9533	3.6164	0.0808	274.5	calc	calc	calc

Table 3-5 The table shows the mean values for the á priori information. The values marked with calc, is calculated using some simpler algorithms (Reference: Comiso et. Al. 1997 and Cavalieri et. Al. 2000)

As described earlier the process of estimating the geophysical parameters is an iterative process. After some investigations it has been decided always to make 5 iterations for each measurement. After the 5th iteration a test value is calculated in order to have a measure of how good the estimation is. The test value is calculated as the square root of the sum of the error for each of the AMSR channels. The error is calculated as the difference between the measured brightness temperature and the brightness temperature calculated by the forward model from the estimated geophysical parameters.

4 Verification

4.1 Comparison of SSM/I vs. AMSR - synthetic data

In order to verify that the model without ice works, a test has been carried out with synthetic data. 4 synthetic data sets, which contain brightness temperatures, have been calculated by the forward model. For each data set one of the geophysical parameters has been varied over an interval, while the rest have been kept on a default value. The default values are shown in Table 4-6.

Parameter	**Default value**
Wind speed [m/s]	8
Water vapor [mm]	10
Liquid water [mm]	0.05
Sea surface temperature [K]	275

Table 4-6 Default parameters used for simulation.

The data sets have been used as input to the inverse function, and finally the difference between the input parameter to the forward function and the estimated parameter has been calculated. The results of the simulation - the difference between the input and output parameter - can be seen for each of the 4 data sets in Figure 4-1, Figure 4-2, Figure 4-3 and Figure 4-4. For reference the simulations have been carried out for synthetic data sets for AMSR and SSM/I (The SSM/I forward model is described by Wentz 1997). Furthermore the standard deviations of the estimates are also showed in the figures.
When looking at the graphs it can be seen, that the estimated parameters are quite accurate and, that they have low standard deviations. When comparing the results from the AMSR model with the results from the SSM/I model it can be seen, that in general the AMSR gives the best result. But, when looking at the sea surface temperatures, the SSM/I model obtains better results than the AMSR model. The explanation for this is probably that the SSM/I do not have the low frequency channels (6 and 10GHz) included, and it is these channels which contains most information about the temperature variations. Therefore the retrieval of the sea surface temperature form the SSM/I data are mostly based on the á priori information. This is discussed further in section 4.3 “Test of exclusion of the 6GHz and 10GHz channels”. Concerning the standard deviation of the liquid water content the SSM/I model also obtains the smallest values.

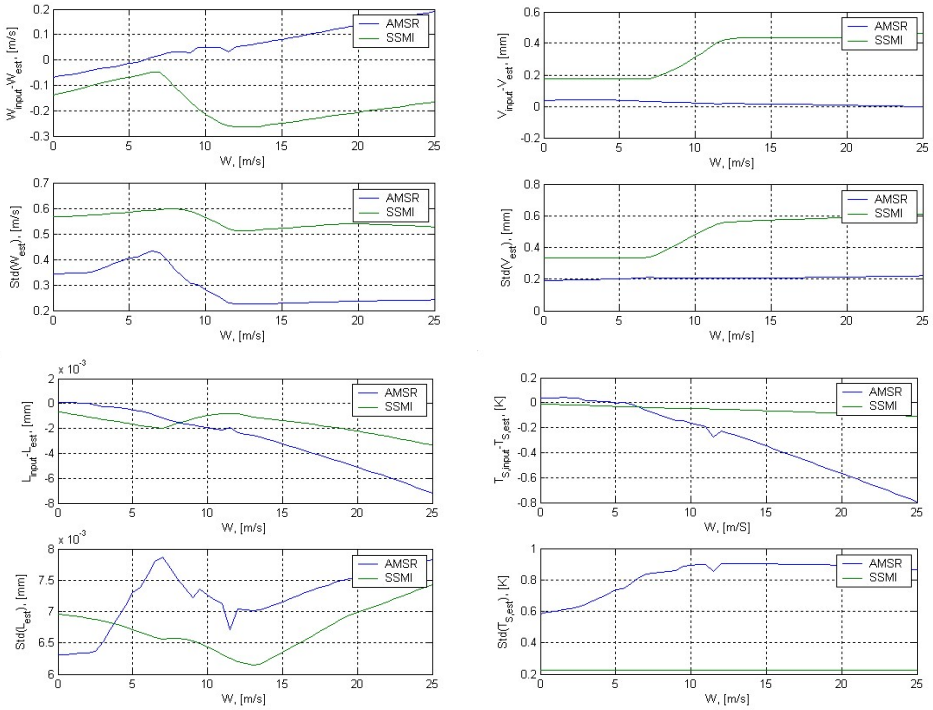

Figure 4-1 Comparison between the geophysical parameters estimated from SSM/I and AMSR data as a function of the wind speed. The figure contains 2 graphs for each parameter. The first graph shows the difference between the input parameter in the forward model and the output parameter from the inverse model. The second graph shows the standard deviation of the estimated parameters.

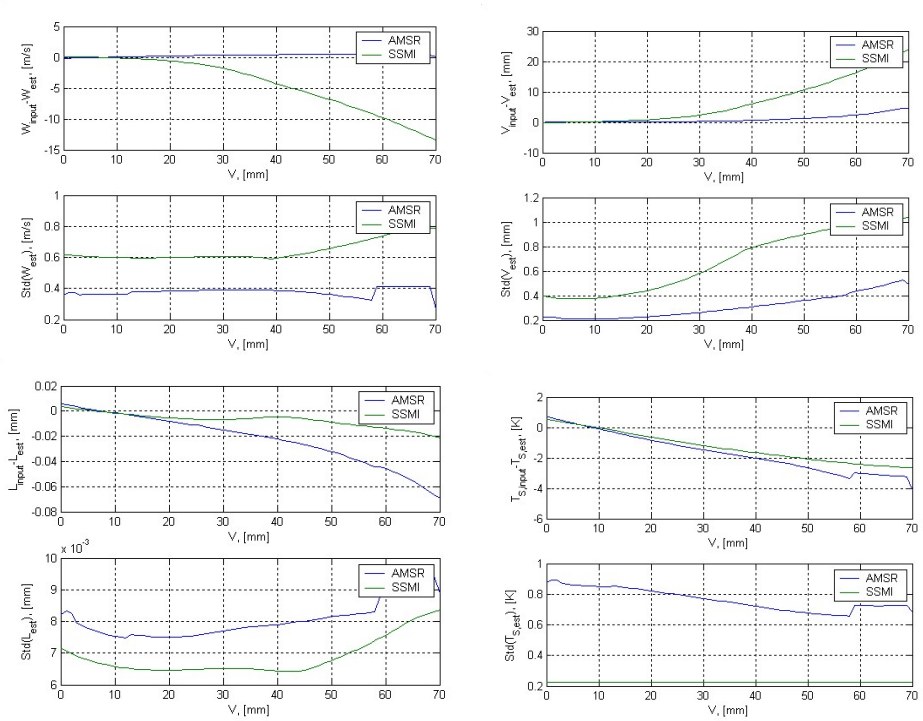

Figure 4-2 Comparison of the geophysical parameters estimated from SSM/I and AMSR data as a function of the water vapor. The figure contains 2 graphs for each parameter. The first graph shows the difference between the input parameter in the forward model and the output parameter from the inverse model. The second graph shows the standard deviation of the estimated parameters.

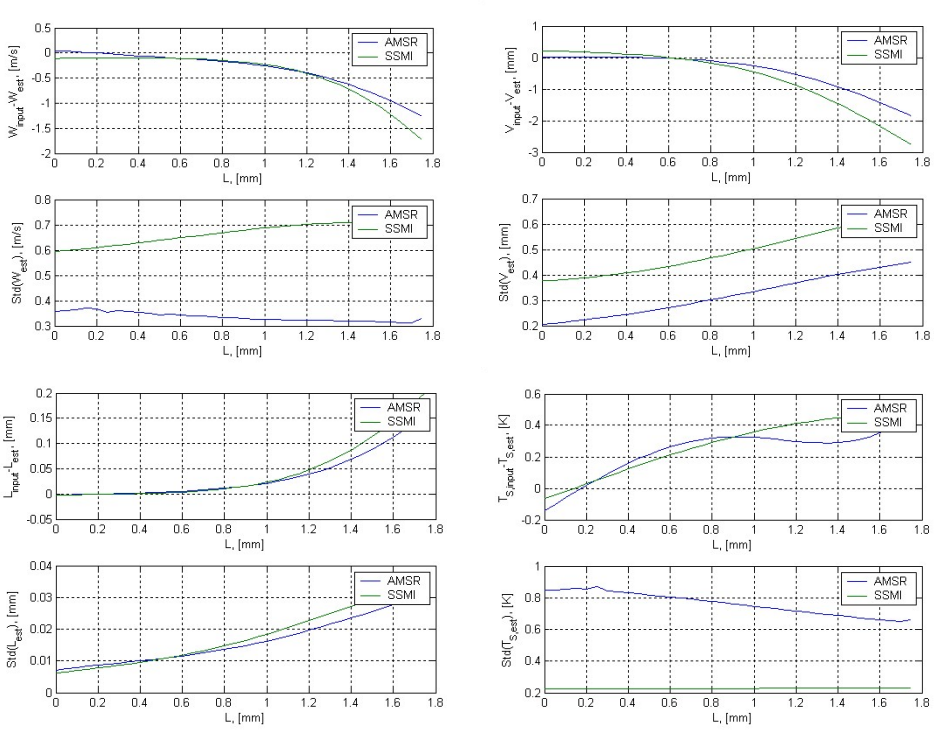

Figure 4-3 Comparison of the 4 geophysical parameters estimated from SSM/I and AMSR data as a function of the liquid water. The figure contains 2 graphs for each parameter. The first graph shows

the difference between the input parameter in the forward model and the output parameter from the inverse model. The second graph shows the standard deviation of the estimated parameters.

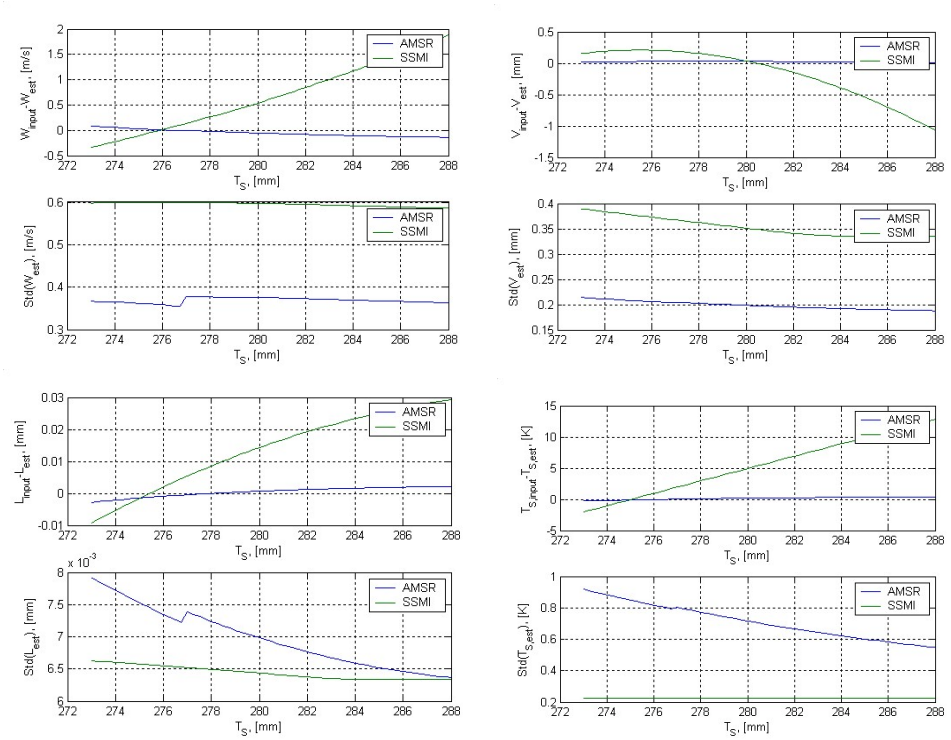

Figure 4-4 Comparison of the 4 geophysical parameters estimated from SSM/I and AMSR data as a function of the sea surface temperature. The figure contains 2 graphs for each parameter. The first graph shows the difference between the input parameter in the forward model and the output parameter from the inverse model. The second graph shows the standard deviation of the estimated parameters.

4.2 Comparison between the model with and without ice

In order to compare the original model and the model, which has ice included; the two algorithms have been tested on a line of data from a satellite passage over the North Atlantic the 18th of November 2003. The data set contains scan element no. 150 and covers both open water and sea ice. The first 100 samples are samples from an ice-covered surface and a little bit of Svalbard. The samples 100 to 250 are measured over open water. The next 25 samples are land (Iceland), and finally the rest of the samples are again measured over open water. The line of data is shown in Figure 4-5. In this figure the line of data is shown on top of an ice concentration image and on top of an image of the amount of liquid water, so it can be seen what the data line contains.

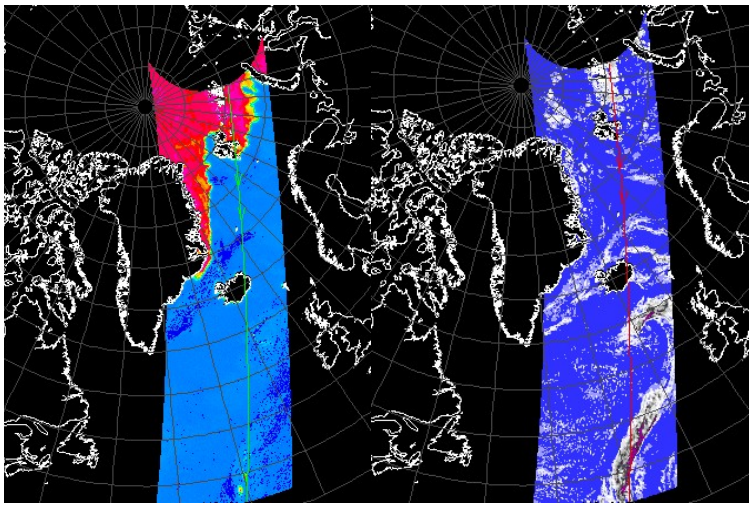

Figure 4-5 To the left is a map of the sea ice concentration, and to the right is a map of the amount of liquid water. On the two maps is the placement of the line of data illustrated as a green or a read line.

The estimated geophysical parameters from the data set are shown on Figure 4-6 to Figure 4-11. For each parameter the estimated value and the standard deviation is shown. When looking at the figures it can be seen, that the wind can not be estimated over the sea ice surface. This is logical because the wind speed is retrieved mainly from the microwave signature of the wind induced sea surface roughness, which is missing over the sea ice. When looking at the wind speed estimated over open water it can be seen, that by including ice in the forward model the standard deviation increases, e.g. the retrieval becomes more uncertain.

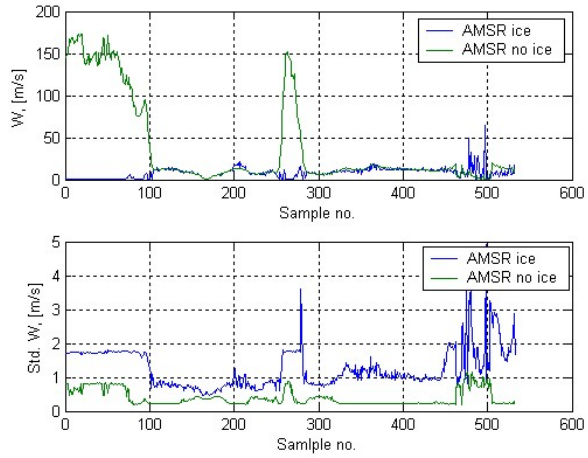

Figure 4-6 The first graph shows the estimated wind speed for the two models, and the second graph shows the standard deviation of the estimated wind speeds.

Looking at the estimated water vapor and liquid water in Figure 4-7 and Figure 4-8, it can be seen, that over open water it does not matter whether ice is included in the model or not. On the other hand, when ice is included in the model, it is possible to estimate the amount of water vapor or liquid water over the ice surface, but with a higher standard

deviation than over the open water surface. Typical Standard deviations of V are 0.3 mm over ocean and 1 mm over ice.

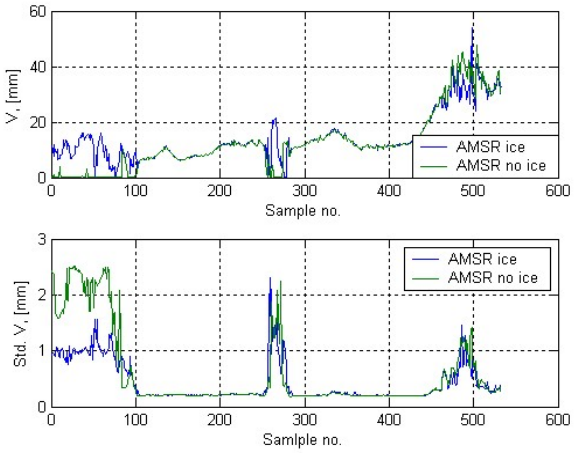

Figure 4-7 The first graph shows the estimated water vapor for the two models, and the second graph shows the standard deviation of the estimated water vapor.

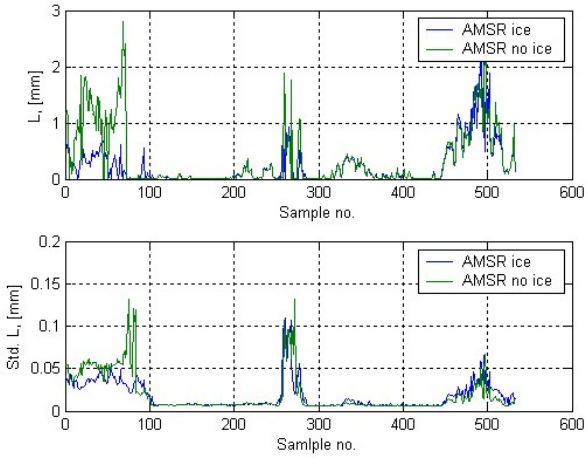

Figure 4-8 The first graph shows the estimated liquid water for the two models, and the second graph shows the standard deviation of the estimated liquid water.

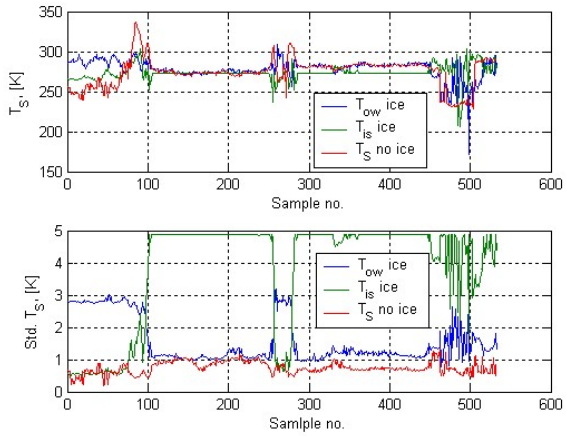

Figure 4-9 The first graph shows the estimated temperatures for the two models, and the second graph shows the standard deviation of the estimated temperatures. The graphs show 3 temperatures because the model with ice contains two temperatures – the ice temperature and the open water temperature – and the model without ice only contains one temperature namely the sea surface temperature (which is the open water temperature).

When considering the surface temperatures in Figure 4-9, it can be seen, that the ice temperature estimated by the original model is not correct. On the other hand when looking at the model with ice, it can be seen, that the temperature of the ice and the temperature of the open water are being estimated correctly according to the surface type. Comparing with the ice concentration it can be seen, that the standard deviation of the two temperatures indicate, which of the temperatures is the correct one representing the current surface type.
Figure 4-10 and Figure 4-11 shows the results of the estimation of the ice parameters, estimated only by the algorithm where ice is included. From the figures it can be seen, that the ice concentration is estimated quite well with a standard deviation of about 1-2%. It is only in the end of the data line (around sample no. 475), that some noise appears; this is due to the large amount of liquid water in the atmosphere at this location (see Figure 4-5). When considering the multi year ice fraction, it can be seen, that over the ice surface the fraction is being estimated quite well. On the other hand over the open water the multi year ice fraction takes strange values, but again this is indicated by an increased standard deviation, and is considered less important since the ice concentration is very low.

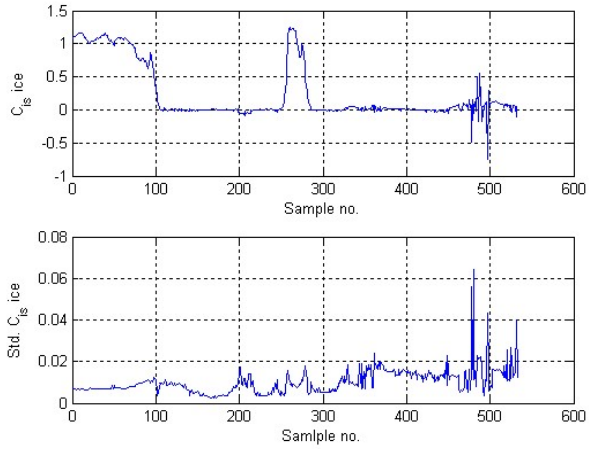

Figure 4-10 The first graph shows the estimated ice concentration for the ice model, and the second graph shows the standard deviation of the estimated ice concentration.

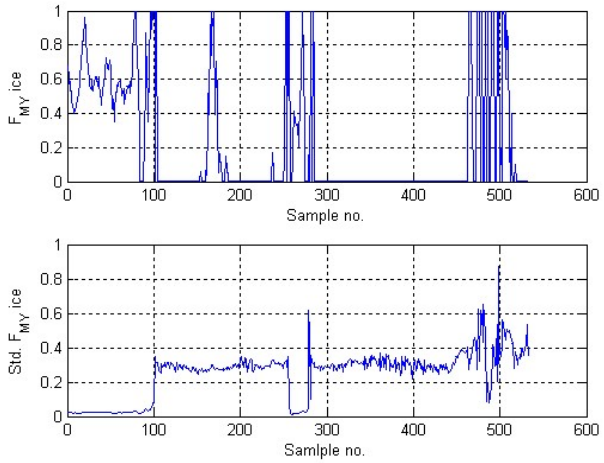

Figure 4-11 The first graph shows the estimated multi year ice fraction for the ice model, and the second graph shows the standard deviation of the estimated multi year ice fraction.

In Figure 4-12 the test value of the estimation is shown. From the test value it is clearly indicated, that the inclusion of ice in the model makes it easier for the model to make the brightness temperatures fit to the geophysical parameters over the ice surface. Furthermore it does not look like the inclusion of ice has influence on the estimation of the geophysical parameters over open water except for the area, which has a high content of liquid water (around sample 475). The increased test value over the cloud of liquid water can not be explained at the moment. We have tried to solve the problem by increasing the amount of iterations, but it did not solve the problem. At the moment we come around the problem by removing the retrieved geophysical parameters, which has a high test value. But of cause the problem should be a topic for further investigations in the future.

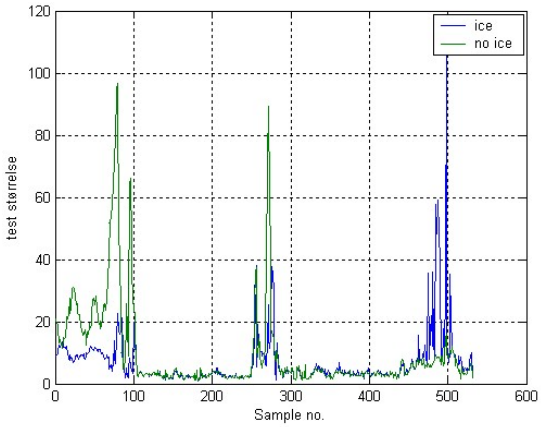

Figure 4-12 Test value.

4.3 Test of exclusion of the 6GHz and 10GHz channels

In order to figure out how much the inclusion of the low frequency channels 6.9GHz and 10.7GHz means for the estimation of the geophysical parameters, a test has been carried out for the same data line as used in the previous section. The test has been carried out for the ice model, and first the exclusion of the 6GHz cannel has been tested, and then the exclusion of both the 6GHz and the 10GHz has been tested.

The way the channels have been excluded from the estimation is by setting the appropriate element in the covariance matrix for the measurements, $\mathbf{S_e}$ to a high value (it has been set to 100000). The result of the test is shown in Figure 4-13 to Figure 4-20. On each of the figures the graphs from the two tests are shown together with the graph for the estimation where all the AMSR channels are included.

For the estimation of the wind speed the exclusion of the low frequency channels only has an influence if there is a lot of water in the atmosphere.

For the estimation of water vapor and liquid water the exclusion of the low frequency channels has a large influence on both the estimation of the parameters and the standard deviation of the estimate over the ice covered surface, but not over the water surface. The error of the estimated parameter and the standard deviation increases when the 6GHz channel is excluded and even more, when both the 6GHz and the 10GHz channels are excluded.

When looking at the sea surface temperatures it has a large influence on the estimated value and on the standard deviation of the open water temperature to exclude the 6GHz channel, but it nearly does not make any differenced also to exclude the 10GHz channel. Concerning the ice surface temperature the standard deviation increases when the low frequency channels are being excluded, but not as much as for the open water temperature. Furthermore the 10GHz channel has an influence on the estimated value.

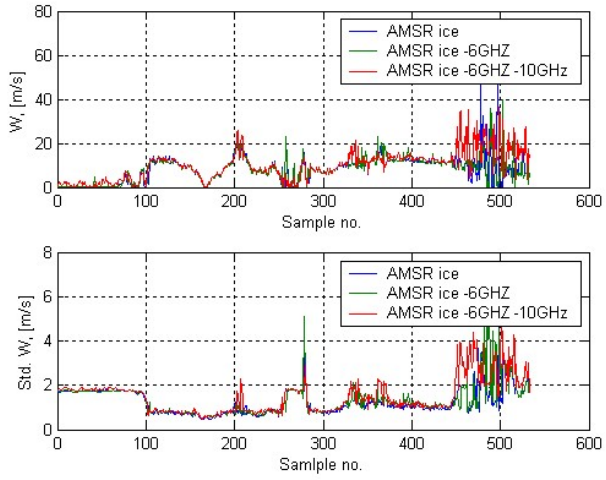

Figure 4-13 Estimate and standard deviation of the wind speed.

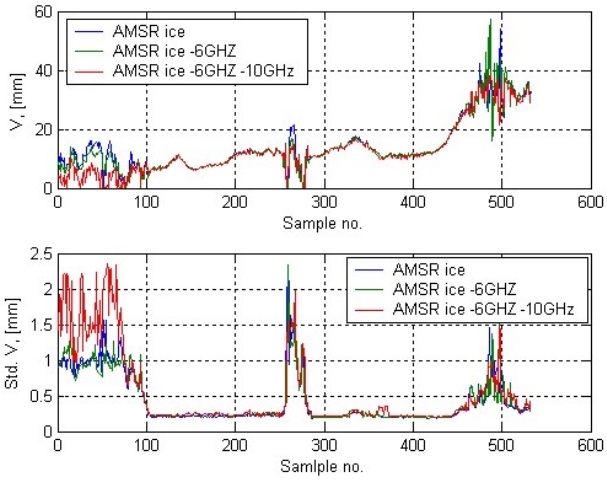

Figure 4-14 Estimate and standard deviation of the water vapor.

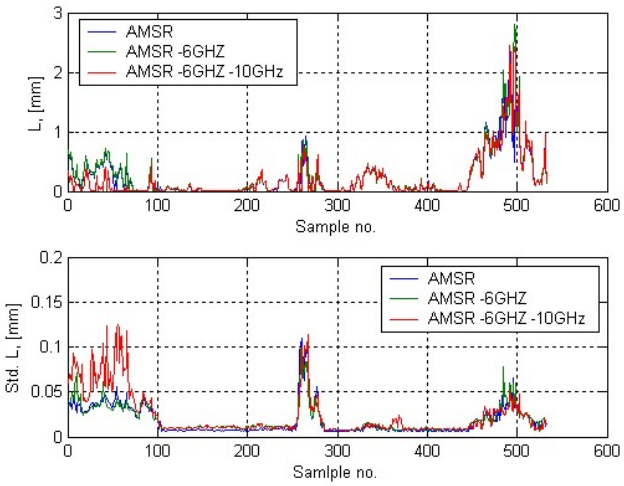

Figure 4-15 Estimate and standard deviation of the liquid water.

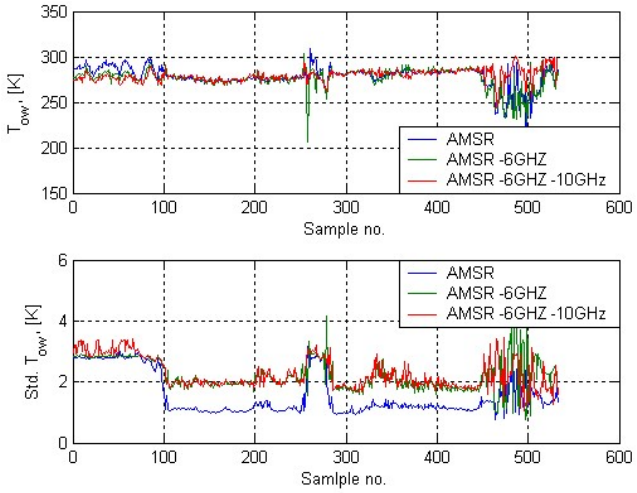

Figure 4-16 Estimate and standard deviation of the open water temperature.

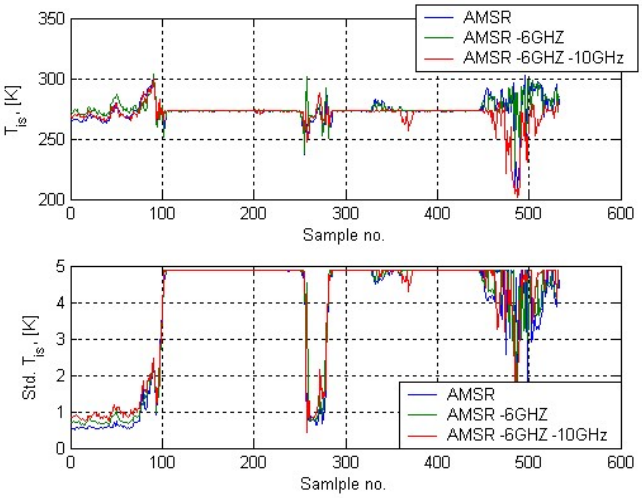

Figure 4-17 Estimate and standard deviation of the sea ice temperature.

For the ice concentration it looks like the removal of the low frequency channels only has an influence on the standard deviation of the result over water, where there is a lot of water in the atmosphere. On the other hand for the multi year ice fraction the exclusion of the low frequency channels has an influence, but as shown on the graph, very little on the standard deviation of the estimate. This is particular true over the ice surface and when there is a lot of water in the atmosphere. When there is a lot of liquid water in the atmosphere the standard deviation of the multi year ice fraction increases.

When considering the test value, one can see that the exclusion of the low frequency channels makes the test value increase especially when there is a lot of liquid water in the atmosphere.

All in all it can be concluded that the low frequency channels have the greatest impact on the estimated parameters and the standard deviation where water and in particular liquid water is present in the atmosphere.

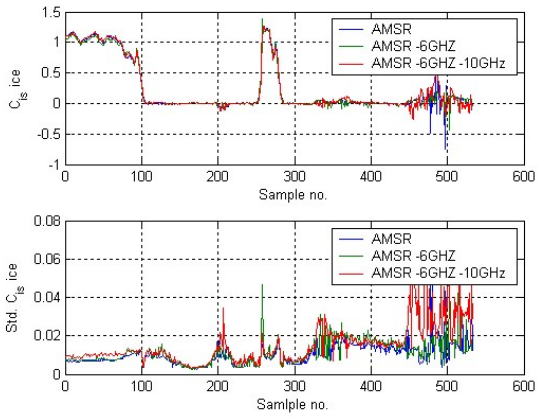

Figure 4-18 Estimate and standard deviation of the sea ice concentration.

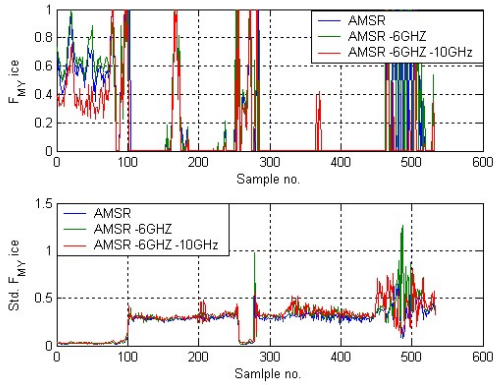

Figure 4-19 Estimate and standard deviation of the multi year ice fraction.

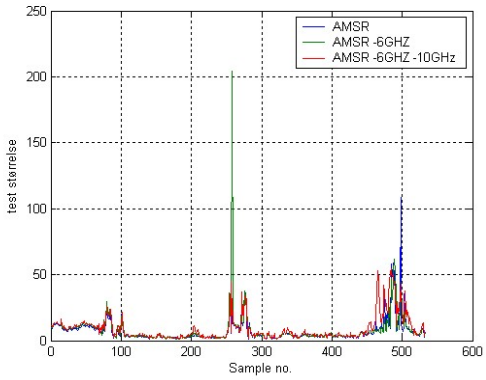

Figure 4-20 Test value.

4.4 Comparison with Wentz data

In order to verify the results obtained by the retrieval algorithm a comparison between our retrieved geophysical parameters and geophysical parameters from Remote Sensing System/Frank Wentz (downloaded from www.remss.com) has been carried out. The comparison for the 18th of November 2003 can be seen in Figure 4-21 to Figure 4-24 for the four geophysical parameters near surface wind speed, water vapor, liquid water and

open water sea surface temperature. The model, which has ice included, has been used for our calculations. It is only the four showed parameters, which can be compared, because Wentz do not have sea ice included in his algorithm.
The four graphs show scatter plots of our geophysical parameters versus the geophysical parameters from Frank Wentz. When considering the four graphs the first thing to be noted is that the data of Frank Wentz is quantized and ours are not (this can be seen in some of the graphs as the vertical stripes in the data clouds).
When comparing the parameters, it can be seen, that there is clear linear relationship for three of the parameters (wind speed, water vapor and sea surface temperature). Concerning the liquid water parameter the linear relationship is not as clear as for the other parameters. For all four parameters the results are placed in a cloud around the x=y line (red line). For the wind speed the cloud of data is almost centered on the x=y line and therefore it looks like the two algorithms have about the same amount of data, which is over and under estimated. When looking at the results of the estimated water vapor, it looks like our algorithm almost always estimates a little more water vapor than the algorithm of Frank Wentz. For the graph of the liquid water it is difficult to see a clear linear relationship, but still all the estimated values are gathered in a cloud. When zooming in on the cloud it shows out, that most of the data is actually gathered around the x=y line, but maybe the data from our calculations have a little higher values than the results of Wentz. Finally, when considering the sea surface temperature, the cloud of data is also centered on the x=y line, but now it is the values of Wentz, which are a little higher than our results.
The mean values of the standard deviations of our calculations are showed in Table 4-7. It has not been possible to find the exact standard deviation for the calculations of the geophysical parameters by Wentz. Instead the table shows the expected standard deviation for the algorithm by Went (Wentz 2000). These standard deviations can contribute to some of the explanations of differences in the geophysical parameters retrieved from our algorithm and from Wentz' algorithm. Furthermore one has to remember, that it was showed 4.2 "Comparison between the model with and without ice", that the inclusion of ice in the algorithm has an influences on the standard deviation of the estimated parameters.

Parameter	**Our mean value of the standard deviation**	**Expected standard deviation for Wentz**
Wind speed [m/s]	1.22 m/s	1.0 m/s
Water vapor [mm]	0.38 mm	1.0 mm
Liquid water [mm]	0.013 mm	0.02 mm
Sea surface temperature [K]	1.48 K	0.5 K

Table 4-7 The table shows the mean of the standard deviation for 4 of the geophysical parameters estimated by our algorithm and the expected standard deviation for the estimation by Wentz (Wentz 2000).

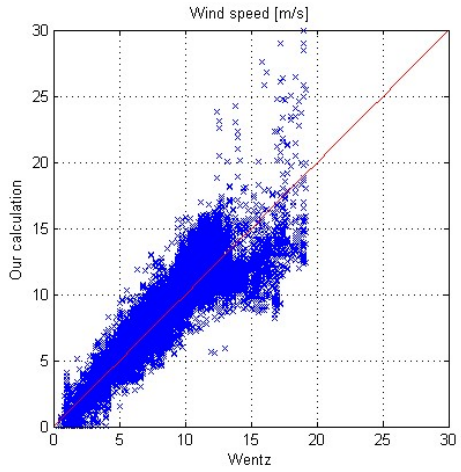

Figure 4-21 Comparison of the near surface wind speed calculated by Wentz and calculated by us. Data is from the 18th of November 2003.

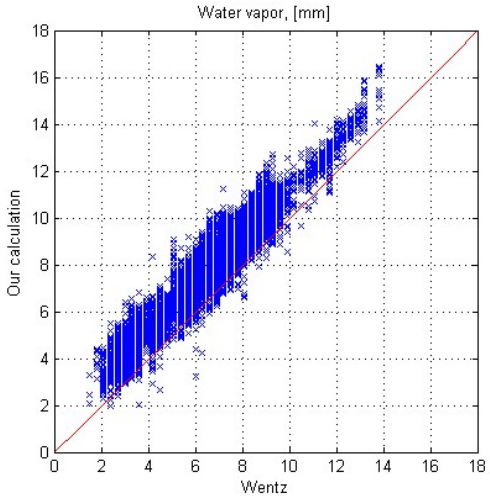

Figure 4-22 Comparison of the water vapor calculated by Wentz and calculated by us. Data is from the 18th of November 2003.

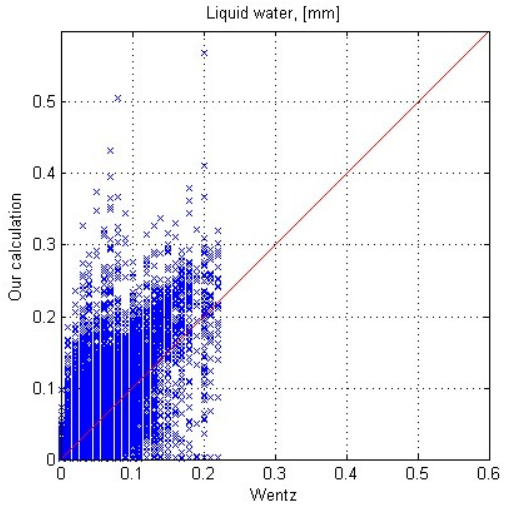

Figure 4-23 Comparison of the liquid water calculated by Wentz and calculated by us. Data is from the 18th of November 2003.

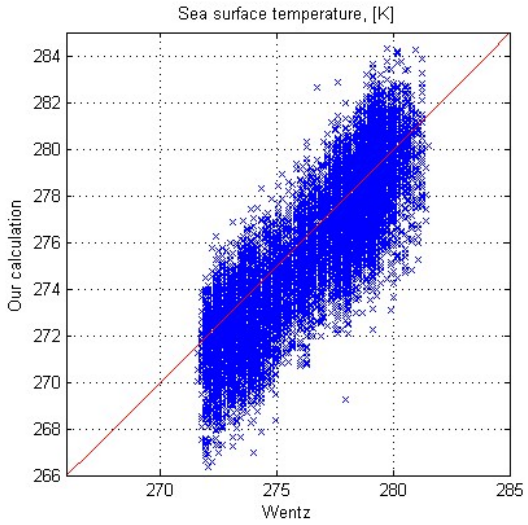

Figure 4-24 Comparison of the sea surface temperature calculated by Wentz and calculated by us. Data is from the 18th of November 2003.

4.5 SST comparison with O&SI SAF data

In order the verify the sea surface temperature (SST) a comparison with Ocean & Sea Ice Satellite Application (O&SI SAF) data has been carried out. The regional SST SAF data are derived form the NOAA/AVHRR data. The data has a resolution of 2 km and is available from the North Atlantic area every 6th hour (Météo-France, 2002).
The sea surface temperature has been compared for data form three different days. The result of the comparison can be seen in Figure 4-25 to Figure 4-27. From the three figures it can clearly be seen, that there is a linear relation ship between the two sea surface temperatures. The standard deviation of the SAF SST is 0.6-0.8K and the standard

deviation for the SST retrieved by our algorithm is about 1.2K, and this might explain some of the variation in the three scatter plots.
In the scatter plots for the data in November there are two clouds of data, which has no linear relationship with the SAF SST. For these data our algorithm has estimated very low values, while the SAF data has values above 273^0K. It our sea surface temperatures, which are estimated wrongly and they occur due to an error in the AMSR radiometer at some scan angles.

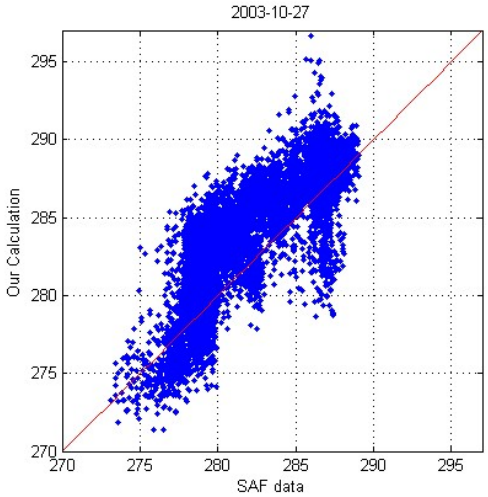

Figure 4-25 Scatter plot of the SAF surface temperature and our calculated surface temperature at the 27th of October 2003.

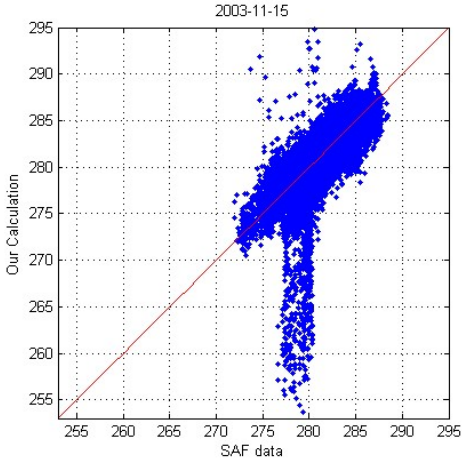

Figure 4-26 Scatter plot of the SAF surface temperature and our calculated surface temperature at the 15th of November 2003.

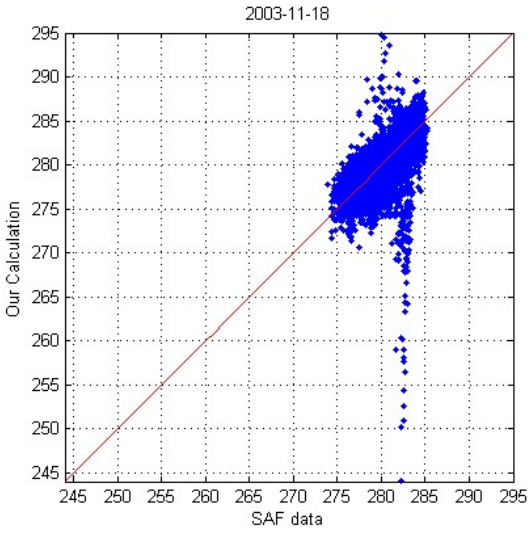

Figure 4-27 Scatter plot of the SAF surface temperature and our calculated surface temperature at the 18th of November 2003.

4.6 Sea ice comparison

In order to find out how well the algorithm estimates the sea ice concentration the results from our algorithm has been compared with results from the NASA Team Sea Ice Algorithm. The comparison has been carried out for two types of data set. The first type of data is one, which contains one line in the AMSR scan at a specific satellite passage. The second type of data is a time series of data from a specific location.

4.6.1 Comparison with line of data

A data set with a line of data from a satellite passage the 18th of November 2003 has been use as an example. The data set is the same as the one described in section 4.2 ”Comparison between the model with and without ice”. The data set contains both an area with open water and an area with sea ice. Some of the area containing open water is covered by a big cloud.
The ice concentration for the data set has been calculated with our algorithm and with the NASA Team Sea Ice Algorithm, and the result can be seen in Figure 4-28. In Figure 4-29 is the standard deviation of the estimated ice concentration by our algorithm showed. When looking at the estimated ice concentrations it can be seen, that the NASA team algorithm estimates a lower concentration than our algorithm over the ice covered area. The ice concentration over this area is expected to be 1, but when the truth concentration is not known exactly, it is not really possible to judge which of the algorithms gives the most correct ice concentration. On the other hand over the open water area the ice concentration is well known to be 0. When looking at the graphs it can be seen that our algorithm gives the most correct ice concentration. This is particularly clear in the area

with the big cloud, where the NASA Team Sea Ice Algorithm calculates ice concentrations as high as 0.5.

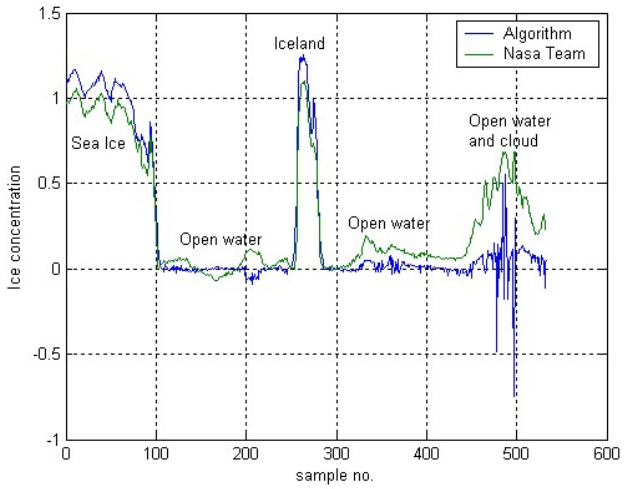

Figure 4-28 Ice concentrations from line of data at the 18th of November 2003.

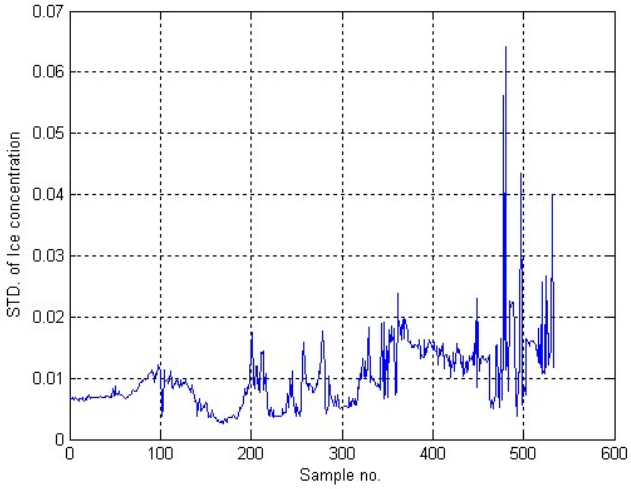

Figure 4-29 Standard deviation from our algorithm.

4.6.2 Time series

The places for the recording of the time series data are showed on the map on Figure 4-30. As examples have the open water areas 50, 51 and 52, the FY area 44 and the MY area 43 been used.

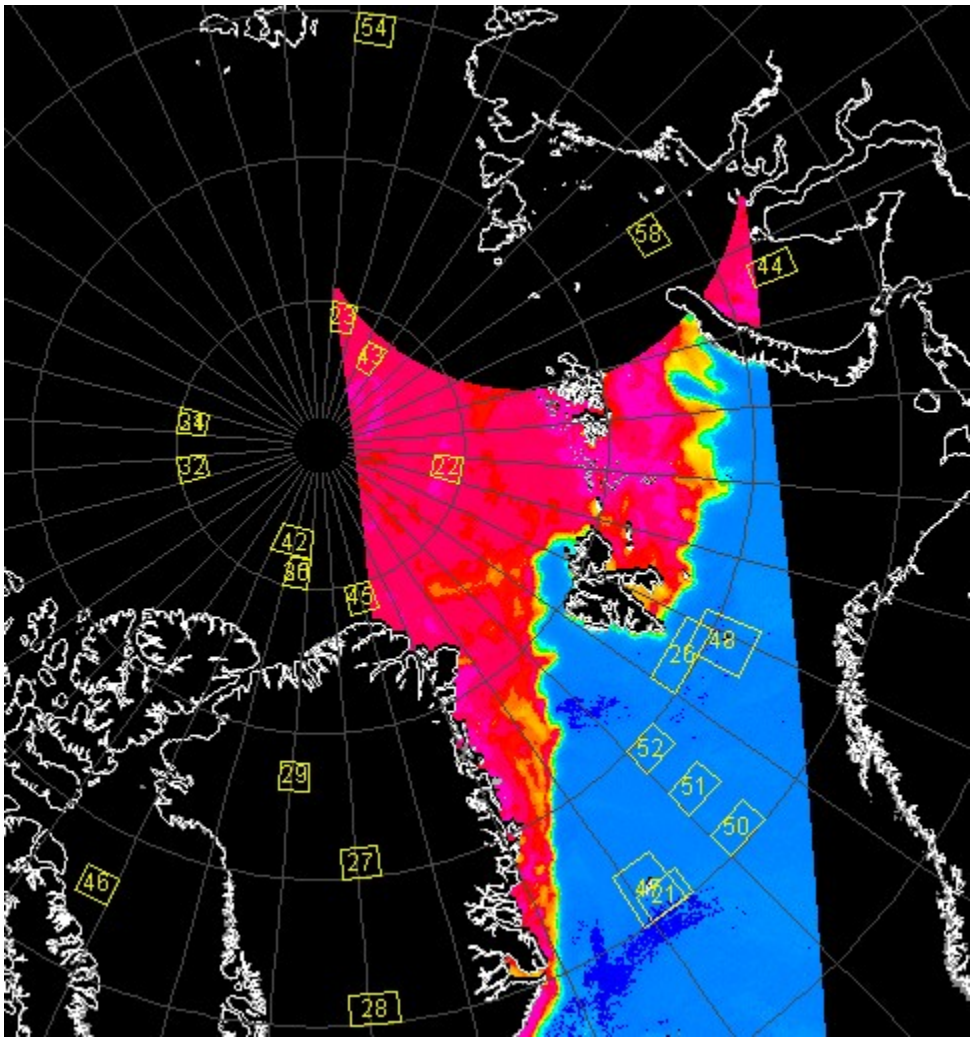

Figure 4-30 The Map shows the time series areas and the estimated ice concentration from the 18th of November 2003.

The results of the calculation over the open water area can be seen on Figure 4-31 to Figure 4-36, and a summary of the results are given in Table 4-6 to Table 4-8. For each of the 3 open water areas are 4 graphs showed. The first one shows the estimated ice concentration for the 2 algorithms. The second one shows the standard deviation for the estimated ice concentration from our algorithm. The last two graphs shows the calculated MY and FY concentration.

When looking at the graphs and the tables it can be seen, that our algorithm gives a better estimate of the ice concentration than the NASA Team Algorithm does, especially concerning the standard deviation. This is also the fact when looking at the estimation of the estimated ice concentration FY and MY ice. The standard deviations for our algorithm calculated from the time series (the one in the table) is, compared with the levels from the algorithm (the second graph), very high. This is because the standard deviation from our algorithm only represents how good the estimate is according to the model, and not how good the model actually is. Therefore the difference between the two standard deviations is a measure of how good the model actually is compared to real life.

When comparing the results form the three open water data set it can be seen that the standard deviation from the time series decreases the further north the data has been collected, this is due to the lower temperature and thereby the lower amount of liquid water the further north one comes.

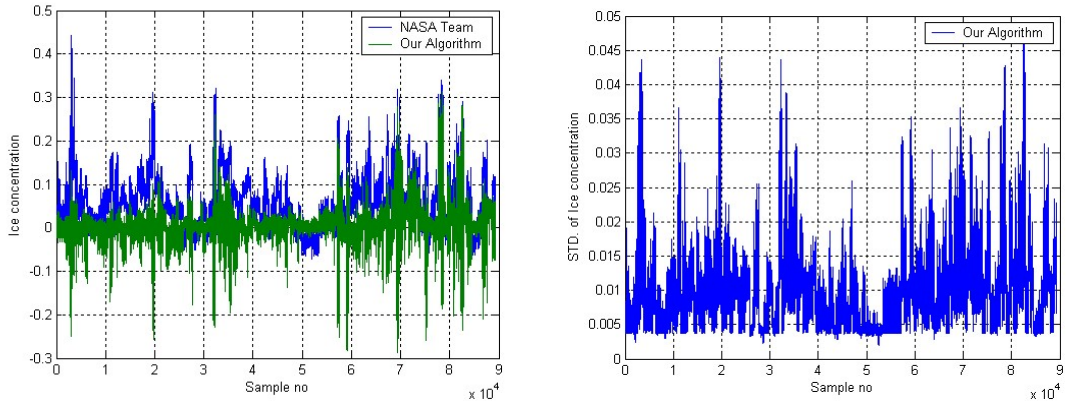

Figure 4-31 The left graph shows the total sea ice concentration for area 50, and the right graph shows the standard deviation from the estimation of the ice concentration by our algorithm.

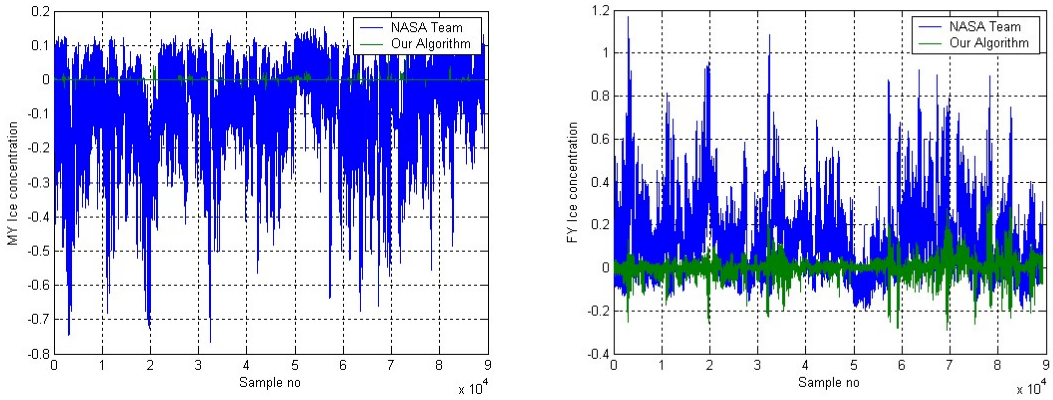

Figure 4-32 The left graph shows the MY ice concentration and the right graph shows the FY ice concentration for area 50.

	Total ice concentration		FY ice concentration		MY ice concentration	
	Mean	Std.	Mean	Std.	Mean	Std.
Our algorithm	0.0123	0.0405	0.0122	0.0404	0.0001	0.0015
NASA Team	0.0636	0.0614	0.1359	0.1648	-0.0722	0.1206

Table 4-8 The table shows the mean and standard deviation for each algorithm for area 50.

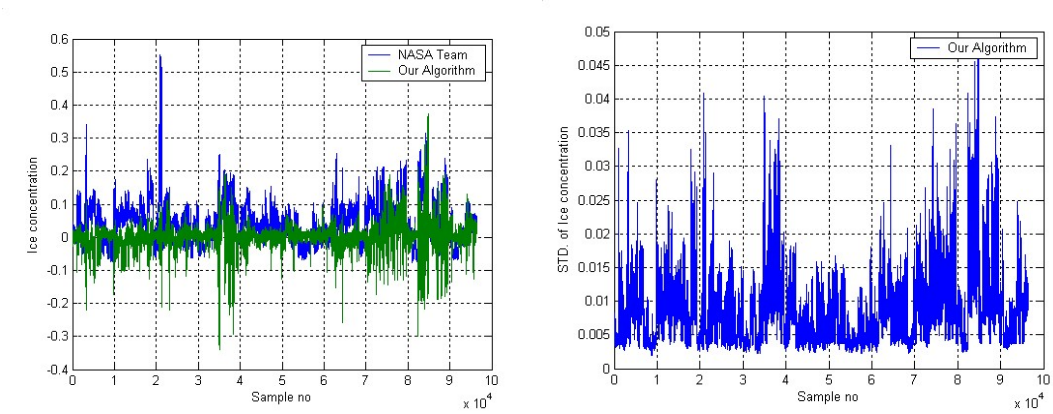

Figure 4-33 The graph shows the total sea ice concentration for area 51. The right graph shows the standard deviation of the ice concentration estimated by our algorithm.

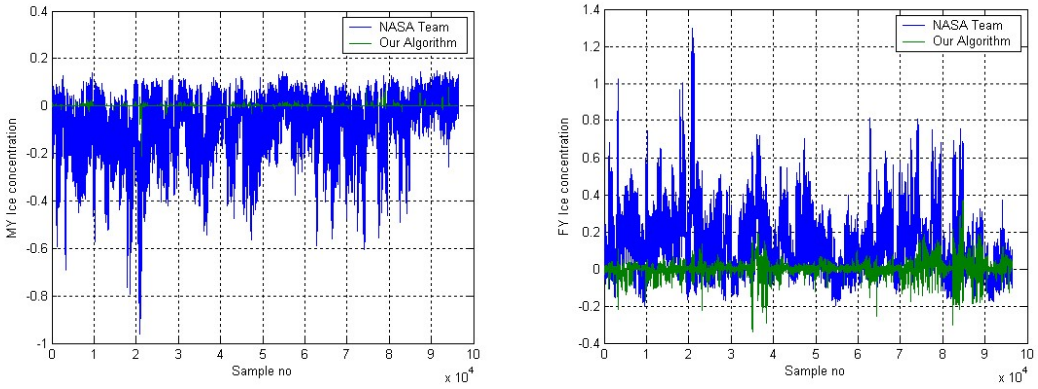

Figure 4-34 The left graph shows the MY ice concentration and the right graph shows the FY ice concentration for area 51.

	Total ice concentration		FY ice concentration		MY ice concentration	
	Mean	Std.	Mean	Std.	Mean	Std.
Our algorithm	0.0088	0.0391	0.0001	0.0042	0.0087	0.0388
NASA Team	0.0527	0.0626	-0.0793	0.1186	0.1320	0.1597

Table 4-9 The table shows the mean and standard deviation for each algorithm for area 51.

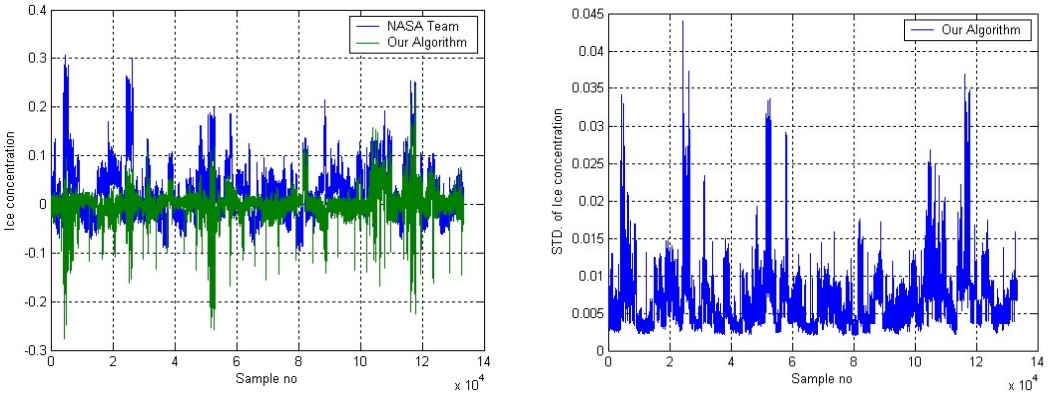

Figure 4-35 The graph shows the total sea ice concentration for area 52. The right graph shows the standard deviation of the ice concentration estimated by our algorithm.

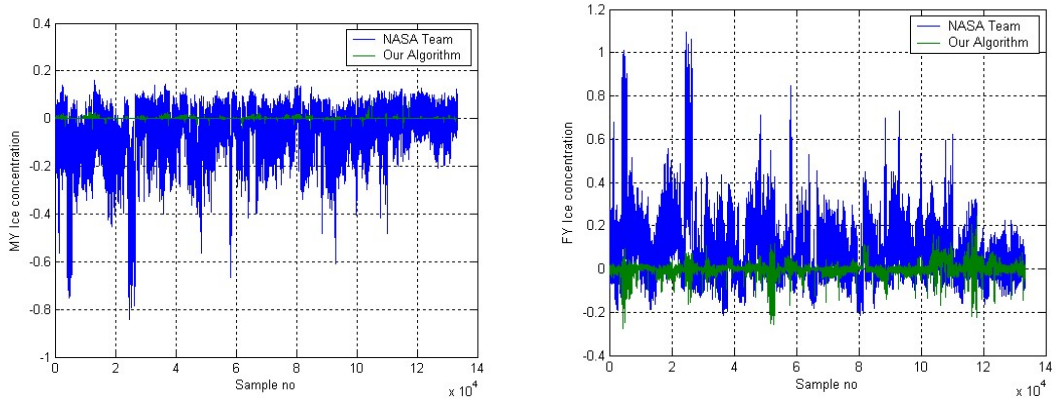

Figure 4-36 The left graph shows the MY ice concentration and the right graph shows the FY ice concentration for area 52.

	Total ice concentration		FY ice concentration		MY ice concentration	
	Mean	Std.	Mean	Std.	Mean	Std.
Our algorithm	0.0018	0.0274	0.0013	0.0269	0.0005	0.0028
NASA Team	0.0274	0.0509	0.0836	0.1302	-0.0563	0.0976

Table 4-10 The table shows the mean and standard deviation for each algorithm for area 52.

In Table 4-11 to Table 4-13 the results for 3 FY areas are showed, and in Table 4-14 and Table 4-15 the results for 2 MY areas are showed. When looking at the results in the tables, it can be seen, that our algorithm always estimates the highest ice concentration and often an ice concentration, which is higher than 1. Furthermore our algorithm estimates more MY ice than the NASA Team algorithm and less FY ice than the NASA Team algorithm. This indicates that the emissivities used in our algorithm are not fully correct, so this might be a subject for further investigations. The standard deviations obtained in the examples are very close to each other for the two algorithms, and thereby indicates that they probably represents some actual variations in the ice concentration.

	Total ice concentration		FY ice concentration		MY ice concentration	
	Mean	Std.	Mean	Std.	Mean	Std.
Our algorithm	1.0726	0.0423	0.3198	0.2321	0.7528	0.2081
NASA Team	0.9797	0.0419	0.8302	0.0997	0.1225	0.0888

Table 4-11 The table shows the mean and standard deviation for each algorithm for area 54 (FY area).

	Total ice concentration		FY ice concentration		MY ice concentration	
	Mean	Std.	Mean	Std.	Mean	Std.
Our algorithm	1.0166	0.1528	0.6524	0.3380	0.3642	0.2878
NASA Team	0.8646	0.1161	0.8177	0.1683	0.0428	0.0780

Table 4-12 The table shows the mean and standard deviation for each algorithm for area 44 (FY area).

	Total ice concentration		FY ice concentration		MY ice concentration	
	Mean	Std.	Mean	Std.	Mean	Std.
Our algorithm	0.9981	0.1273	0.6806	0.2960	0.3175	0.2801
NASA Team	0.8333	0.1214	0.7157	0.1586	0.1177	0.0701

Table 4-13 The table shows the mean and standard deviation for each algorithm for area 46 (FY area).

	Total ice concentration		FY ice concentration		MY ice concentration	
	Mean	Std.	Mean	Std.	Mean	Std.
Our algorithm	1.0152	0.0673	0.2034	0.1515	0.8118	0.1095
NASA Team	0.9220	0.0599	0.3179	0.1214	0.6041	0.0987

Table 4-14 The table shows the mean and standard deviation for each algorithm for area 23 (MY area).

	Total ice concentration	FY ice concentration	MY ice concentration

	Mean	Std.	Mean	Std.	Mean	Std.
Our algorithm	1.0337	0.0421	0.1193	0.1132	0.9144	0.0964
NASA Team	0.9527	0.0492	0.3853	0.0911	0.5674	0.0782

Table 4-15 The table shows the mean and standard deviation for each algorithm for area 43 (MY area).

5 Conclusion

A computer efficient forward model for ocean/sea-ice and the atmosphere has been implemented and tested. The model is computationally fast and testing shows that it can be inverted with a stepwise linear inversion to produce as good or better better results than normal sea ice concentration algorithms. In addition the model allows retrieval of a number of atmospheric and ocean surface parameters. The model needs tuning to the actual ice signatures, and a more complete approach will require that the simple ice surface model be replaced by a full ice/snow model as is the purpose of further work in the IOMASA project.

6 References

Cavalieri, Donald J. and Josefino C. Comiso. Algorithm Theoretical Basis Document (ATBD) for the AMSR-E Sea Ice Algorithm. Laboratory for Hydrospheric Processes, NASA Goddard Space Flight Center, Maryland. December 1, 2000

Comiso, Josefino C.; Donald J. Cavalieri; Claire L. Parkinson and Per Gloersen. Passive microwave algorithms for sea ice concentration: A comparison of two techniques. Remote Sens. Environ., Vol 60:357-384, 1997

Météo-France. Ocean & sea Ice SAF. North Atlantic Regional Sea Surface Temperature, Product Manual. Version 1.2. October 2002

NASDA. AMSR-E Data Users Handbook. Technical Report NCX-030021. 1st Edition. July 2003.

Pedersen, Leif Toudal. Retrieval of sea ice concentration by means of microwave radiometry. Technical Report LD81, EMI, The Technical University of Denmark, Lyngby, Denmark, February 1991.

Rodgers, C.D. Retrieval of atmospheric temperature and composition from remote measurements of thermal radiation. Reviews of Geophysics and Space Physics. Vol. 14(nr. 4): 609-624, November 1976.

Wentz, Frank J. A model function for ocean microwave brightness temperatures. Journal of Geophysical Research. Vol. 88(nr. C3): 1892-1908. 1983.

Wentz, Frank J. and Thomas Meissner. AMSR Ocean Algorithm. Algorithm Theoretical Basis Document (ATBD). Remote Sensing Systems. California, U.S. Version 2. November 2. 2002.

Wentz, Frank J. and Thomas Meissner. AMSR Ocean Algorithm. Algorithm Theoretical Basis Document (ATBD). Remote Sensing Systems. California, U.S. Version 2. November 2. 2002.